Loss of *Cxcr2* in myeloid cells promotes tumour progression and T cell infiltration in invasive bladder cancer

Running title: *Cxcr2* loss promotes bladder cancer progression

Nur Faezah Binti Ismail[a], Mona Foth[a,b], Amal Rahil Elgaddafi Yousef[a], Ningxuan Cui[a], Joshua D.G. Leach[b,d], Thomas Jamieson[b], Saadia A. Karim[b], Jonathan M. Salmond[c], Jennifer P. Morton[b,d], and Tomoko Iwata[a*]

[a]School of Medicine, Dentistry and Nursing, College of Medical, Veterinary and Life Sciences, University of Glasgow, Glasgow, UK

[b]Cancer Research UK Beatson Institute, Glasgow, UK

[c]Department of Pathology, Queen Elizabeth University Hospital, Glasgow, UK

[d]Institute of Cancer Sciences, College of Medical, Veterinary and Life Sciences, University of Glasgow, Glasgow, UK

*Correspondence to:

Dr Tomoko Iwata, PhD

Medical Genetics and Pathology, Laboratory Medicine, Queen Elizabeth University Hospital, 1345 Govan Road, Glasgow, G51 4TF, UK.

Tel.: +44 (141) 354 9438

Fax: +44 (141) 232 7991

Email: Tomoko.Iwata@glasgow.ac.uk

Abstract.

BACKGROUND: CXCR2 is a chemokine receptor expressed in myeloid cells, including neutrophils and macrophages. Pharmacological inhibition of CXCR2 was shown to sensitize tumours to immune checkpoint inhibitor immunotherapies in some cancer types.

OBJECTIVE: To investigate the effects of *CXCR2* loss in regulation of tumour-infiltrating myeloid cells and their relationship to lymphocytes during bladder tumorigenesis.

METHODS: Urothelial pathogenesis and immune contexture was investigated in an OH-BBN model of invasive bladder cancer deleted with *Cxcr2* in myeloid cells (*LysMCre* *Cxcr2*$^{flox/flox}$). *CXCR2* gene alterations and expression in human muscle invasive bladder cancer were analysed in The Cancer Genome Atlas.

RESULTS: Urothelial tumour pathogenesis was significantly increased upon *Cxcr2* deletion compared to *wildtype* mice. This was associated with a suppression of myeloid cell infiltration in *Cxcr2*-deleted bladders shortly after the carcinogen induction. Interestingly, following a transient increase of macrophages at the outset of tumour formation, an increase in T cell infiltration was observed in *Cxcr2*-deleted tumours. The increased tumour burden in the *Cxcr2*-deleted bladder was largely independent of T cells and the status of immune suppression. The *Cxcr2*-deleted mouse model reflected the low *CXCR2* mRNA range in human bladder cancer, which showed poor overall survival.

CONCLUSIONS: In contrast to previous reports of increased CXCR2 signalling associated with disease progression and poor prognosis, CXCR2 was protective against bladder cancer during tumour initiation. This is likely due to a suppression of acute inflammation. Sensitization of checkpoint immunotherapy by CXCR2 inhibition in bladder cancer may require an examination of an immune suppressive status.

Keywords; urinary bladder neoplasms, animal models, chemokine receptors, tumour infiltrating lymphocytes, immunosuppression

INTRODUCTION

According to GLOBOCAN data, 550,000 newly diagnosed cases and 200,000 cases of mortality were reported for bladder cancer in 2018, which equates to 3.0% and 2.1% of all cancers, respectively [1, 2]. Bladder cancer is more frequent in males than females and 90% of newly diagnosed cases are in people over 55-years old. More than 80% of the cases are attributed to preventable causes, such as smoking and occupational exposure to carcinogens [2]. Bladder cancer is classified as non-muscle invasive (NMIBC), muscle invasive (MIBC) and metastatic bladder cancer [3]. NMIBC recurs frequently, and the risk of disease progression cannot be undermined [4]. MIBC is treated by neoadjuvant chemotherapy and radical cystectomy, however few management options are available for the metastatic disease, which has dismal prognosis [5]. The burden of bladder cancer is high due to the needs of surveillance and the treatment cost of NMIBC [1]. With the recent uptake of immune checkpoint inhibitor (ICI) immunotherapy in advanced disease, the overall management cost of bladder cancer may further increase by the population growth and ageing [1].

The ICI immunotherapy has been successfully used in the treatment of advanced BC [6-8]. The ICIs restore cytotoxic and proliferative T cell functions by blocking T cell receptor-mediated immune suppressive signalling [6, 7]. The main challenges are relatively low response rates (13-48%), immune-related adverse effects and pseudo-progression [6]. The response is regulated by multiple mechanisms, including the levels of tumour antigens, PD-L1 expression in tumour and immune cells, the level and location of tumour infiltrating lymphocytes (TILs), and the factors that influence TILs, such as cytokine and chemokine

production [6-8]. Approaches to increase tumours' sensitivity to ICI immunotherapy is being intensively studied, including modulation of myeloid cells, such as neutrophils and tumour-associated macrophages (TAMs) [3].

Neutrophils are myeloid cells that account for 50-70% of the total circulating leukocytes, and normally act as the first responder to damaged and inflamed tissues, but are also involved in all stages of cancer progression, including metastasis [9-13]. Neutrophils could play both anti- and pro-tumour roles. A high level of both CD66b neutrophils and CD3 T cells was associated with better overall survival and progression-free survival [14]. Conversely, a high level of tumour infiltrating neutrophils was associated with poor prognosis in both NMIBC and MIBC [15, 16]. A high neutrophil-to-lymphocyte ratio (NLR), a parameter based on the blood level of neutrophils and lymphocytes, is a poor prognosis in many cancers, including bladder cancer [17-20]. Similarly, macrophages could bear an anti- and pro-tumour role, but in the tumour, they are mostly considered as pro-tumour "M2" macrophages and associated with poor prognosis [21-23]. Macrophages play a role in tumour initiation and progression by creating a paracrine and autocrine loop with tumour cells, causing inflammation, angiogenesis, and immunosuppression [22, 23]. In the bladder, macrophages are mostly resident in the submucosa and shown to have detrimental effects on adaptive immunity in both non-malignant and malignant diseases [21, 24].

CXCR2 is a G-protein coupled receptor that binds to chemokines known as glutamic acid-leucine-arginine (ELR)-positive chemokines (CXCL1-3, CXCL5-8), and transmigrates cells to the sites of inflammation [25, 26]. CXCR2 is reported to be expressed on the cell surface of myeloid cells, including neutrophils, monocytes, macrophage, and mast cells [25, 26]. In cancer, its role was mostly reported as pro-tumorigenic [25, 26]. Importantly, CXCR2

inhibition was shown to counteract immunosuppressive myeloid cell populations in the tumour, promoting tumour infiltration of T cells and sensitising tumours to ICI immunotherapy [27, 28]. In the bladder, increased expression of CXCR2 ligands, CXCL5 and CXCL2, was associated with higher tumour grade and worse prognosis [29, 30]. Expressed in bladder cancer cell lines, CXCL5 upregulated metalloproteinase (MMP) 2/9 and induced cell migration and invasion in a CXCR2-dependent manner [29]. CXCR2 and its ligands were also shown to be expressed in and myeloid derived suppressor cells (MDSCs) and activated their migration [30, 31].

The environmental signals coming from the host and the tumour immune microenvironment can regulate the heterogeneous nature of the myeloid cell population. Therefore, the role and the effects of tissue-infiltrating myeloid cells require an investigation in an organ and context-specific manner. Here we have characterised the role of *Cxcr2* during bladder pathogenesis using genetic ablation of *Cxcr2* in myeloid cells in a model of invasive bladder cancer induced by the bladder-specific carcinogen, N-butyl-N-(4- hydroxybutyl) nitrosamine (OH-BBN). *CXCR2* gene alteration and transcript levels in human bladder cancer were further analysed in The Cancer Genome Atlas (TCGA) Cell 2017 dataset [32].

MATERIALS AND METHODS

Mice and carcinogen treatment

Animal experiments were carried out at the CRUK Beatson Institute, Glasgow, in accordance with the Home Office Animal (Scientific Procedures) Act 1986 in the UK (Project Licence 70/9028), adhered to ARRIVE guidelines, and approved by the University of Glasgow

Animal Welfare and Ethical Review Board. Genotyping was performed by Transnetyx (Cordoba, TN, USA). The number of mice used, including gender, is presented (Table 1) and specified in each figure. *LysMCre Cxcr2*$^{flox/flox}$ (*Cxcr2 flox*) mice were generated by crossing *LysMCre* [33] and *Cxcr2*$^{flox/flox}$ mice [28] in C57Bl/6J background. The C57Bl/6J mice (*wildtype*) purchased from Charles River (Tranent, UK) were used as controls. Mice aged 8-10 weeks were administered with 0.05% v/v N-butyl-N-(4- hydroxybutyl) nitrosamine (OH-BBN, TCI, Oxford, UK) in drinking water for 10 weeks (Figure 1A). The bladders of *wildtype* mice aged beyond 20 weeks were monitored using the Vevo3100 ultrasound system with 25-55MHz transducer (Fujifilm VisualSonics, Toronto, Canada) and culled when they showed clinical signs of bladder tumours. Blood was sampled in EDTA-containing tubes and white blood cell populations were analysed using ProCyte Dx Hematology Analyzer (IDEXX, Westbrook, Maine, USA).

Histology, scanning and histopathological scoring

The bladders were dissected and gently emptied of urine by pressing the tissue with forceps. The bladders were fixed in 10% neutral-buffered formalin overnight and embedded in paraffin. Four-μm sections were used for haematoxylin and eosin (H&E) staining and immunohistochemistry (IHC). Stained slides were scanned by NanoZoomer S60 and analysed by NDP View 2 (Hamamatsu, Shizuoka, Japan) or QuPath version 0.2.3 [34]. H&E images were used for histopathological analysis of bladder and tumour phenotype. The scoring criteria are described in Figure 1 legend and Table S1. Scoring was performed by multiple observers (NFBI, NC, MF, TI) in discussion with the pathologists (JMS, JDGL).

Immunohistochemistry

Antigen retrieval (AR) was performed in heat-induced epitope retrieval (HIER) buffer (ThermoFisher Scientific, Waltham, Massachusetts, USA) by microwave to boiling for 1 min at full power, followed by 10 min at 20% power. Sections were incubated with 3% H_2O_2 for 15 minutes and blocked with 2.5% normal goat or horse serum (Vector Laboratories, Peterborough, UK) for 30 minutes. Primary antibody was applied for 1 hour at room temperature. After washing with TBST (VWR, Lutterworth, UK), secondary antibodies (ImmPRESS HRP Polymer Detection Kit, Vector Laboratories) were applied for 30 minutes. Immunoreactivity was detected by 3,3'-diaminobenzidine (DAB) substrate (Vector Laboratories) and slides were counterstained with haematoxylin. Details of the antibodies used are provided in Table S2.

Image analysis

Manual annotation in QuPath [34] was used to measure the area of the carcinoma *in situ* (*CIS*) and tumour. The immune cells stained positively by IHC was quantified in 10 fields of 100 x 100-μm, randomly placed in the urothelium, stroma, muscle layer, and tumour. The mean value was used to represent each sample. QuPath was also used for quantification of $Ki67^+$ and $Caspase3^+$ cells. The stain vector was first adjusted by selecting a representative area indicating haematoxylin and DAB. Region of interest (ROI) was drawn manually for area representing tumour. The mean size of the ROIs was 1.42 mm^2, ranging from 0.18 – 10.00 mm^2. Caspase 3^+ cells were quantified manually using QuPath. For Ki67, positive cell detection command was used. The threshold 1+ on the score compartment "Nucleus: DAB OD mean" was used to categorize positive or negative cells by adjusting the value in each

image. For quality control, all images were also manually scored in the test ROIs. Scoring was performed by at least two independent observers (NFBI, AREY, NXC and TI).

Total RNA extraction and cDNA synthesis

At dissection, the bladder tissue was halved at the midline. One half was processed in paraffin for histology, the other half was collected in RNAlater (Qiagen, Manchester, UK) for RNA extraction and stored at -20°C. The total RNA was extracted using the RNeasy Mini Kit (Qiagen) and was quantified using NanoDrop Microvolume Spectrophotometer (ThermoFisher Scientific). Samples with 260/280 absorbance ratio between 1.8 and 2.2 were used. The integrity of the RNA was also evaluated by agarose gel electrophoresis. RNA samples with two sharp bands, corresponding to 28S and 18S ribosomal RNA, and with the intensity ratio of the 28S:18S = 2:1, were considered intact and used for the further analysis. The RNA samples were stored at -20°C or -80°C. For the cDNA synthesis, 0.5 μg of total RNA was subjected to the removal of genomic DNA elimination and reverse transcription using the RT^2 First Strand Kit (Qiagen). Genomic DNA was removed by incubating 0.5 μg of the total RNA in Buffer GE with a final volume of 10 μl at 42°C for 5 minutes. The reverse-transcription was performed with Buffer BC3, Control P2, RE3 Reverse Transcriptase Mix and RNAse free water added to a final volume of 20 μl and at 42°C for 15 minutes. The reaction was terminated by incubation at 95°C for 5 minutes and added with 91 μl of RNAse-free water, to achieve the final volume of 111 μl. The resultant cDNA was stored at -20°C or used immediately for RNA array.

RNA array

RNA array experiment was performed using RT^2 Profiler Mouse Cancer Inflammation & Immunity Crosstalk PCR Array (Qiagen). The PCR component mix was prepared with 1350 µl of 2X RT^2 SYBR Green Mastermix, 102 µl of cDNA synthesis reaction and RNase-free water added to the final volume of 2700 µl. For each well of the RT^2 Profiler PCR array, 25 µl of the PCR components mix was added. PCR reaction was performed using the StepOnePlus Real-Time PCR System (ThermoFisher Scientific). Thermal cycle conditions were 95°C for 10 minutes, followed by 40 cycles of 95°C for 15 seconds and 60°C for 1 minute. Fold changes between samples were determined using the $2^{-\Delta\Delta CT}$ method. Total RNA from *wildtype* (n= 3) and *Cxcr2 flox* (n=2) bladders at 20 weeks were used. The ΔCT values of house-keeping gene was subtracted from those of each gene, then the mean value for *wildtype* and *Cxcr2 flox* was determined. The ΔΔCT value was determined by ΔCT (*Cxcr2 flox* mean) - ΔCT (*wildtype* mean), then converted to log2 fold by $2^{-\Delta\Delta CT}$.

TCGA data analysis

The clinical information, genomic alternations, mRNA expression, and MIBC molecular Subtype (mRNA Cluster) of human bladder cancer (TCGA, Cell 2017) (n=412) were downloaded from cBioPortal (http://www.cbioportal.org/public-portal/index.do) and from the reference [32].

Statistics

GraphPad Prism 9 (GraphPad Software, San Diego, CA, USA) was used. Gaussian distribution of the data was first evaluated. The differences of the means between two data groups were evaluated using the Mann-Whitney test for non-parametric distributions.

Kruskal-Wallis test was used to evaluate the differences of more than three data groups. Pearson (parametric) or Spearman (non-parametric) tests were used for evaluation of correlation. Overall survival was estimated using the Kaplan–Meier method and analysed using the log-rank test. A p value of <0.05 was considered significant.

RESULTS

Cxcr2 deletion enhanced urothelial tumorigenesis

Using the previously established 10-weeks on, 10-weeks off protocol of OH-BBN induction of invasive urothelial carcinoma [35], we have compared the bladder pathogenesis in mice deleted with *Cxcr2* in the myeloid cell lineage, *LysMCre Cxcr2*$^{flox/flox}$ (*Cxcr2 flox*) and *wildtype* mice at the timepoints of 2, 16 and 20 weeks from the start of carcinogen treatment (Table 1, Figure 1A). Human Protein Atlas data showed that *CXCR2* expression can be detected in many immune cells and is enriched particularly in granulocyte lineage and neutrophils (Protein Atlas version 21.0, https://www.proteinatlas.org/ENSG00000180871-CXCR2)[36]. *LysMCre* mice were previously shown to drive *Cre-lox* recombination in the majority of neutrophils and macrophages, as well as dendritic cells to some extent [33]. The current model is therefore designed to allow evaluation of the effects of *Cxcr2* loss in recruitment of myeloid cells to the bladder tissue, where inflammation was induced by OH-BBN.

Evaluating the tissue histopathology, *Cxcr2 flox* mice showed more frequent occurrence of bladder tumours (p=0.005), higher invasiveness of tumour cells (p=0.025) and squamous transformation (p=0.001) compared to *wildtype* mice at 20 weeks from the start of OH-BBN

treatment (Figure 1B, N-P). The tumour area was similar (mean; *wildtype* 9.2 mm^2, *Cxcr2 flox* 10.4 mm^2, n=15 per genotype) (Figure 1Q). *Cxcr2 flox* bladders showed formation of carcinoma *in situ* (*CIS*) and increased invasiveness at 16 weeks, while *wildtype* bladders remained unchanged (Figure 1C, D, R-T). At 2 weeks, the urothelium of *Cxcr2 flox* and *wildtype* was morphologically indistinguishable (Figure 1E, F). Absence of $Cxcr2^+$ myeloid cells were evident in tumours, the urothelium and around the blood vessels in *Cxcr2 flox* mice (Figure 1G-M). Female *Cxcr2 flox* mice also showed more advanced bladder phenotype compared to *wildtype* females (Figure S1). The phenotype was overall more advanced in males than female mice (Figure 1, S1). Male mice were used in further investigations.

Altogether, *Cxcr2* deletion in myeloid cells led to a significant increase in bladder tumorigenesis, with an earlier and more frequent occurrence of tumours with morphological appearances indicative of enhanced progression.

Effects of Cxcr2 deletion in tissue infiltration of immune cells

We next investigated how *Cxcr2* deletion influenced the tissue infiltration of immune cells. At 2 weeks timepoint, acute inflammation is normally observed in response to OH-BBN treatment [35]. As expected, infiltration of neutrophils, assessed by the canonical IHC markers, including Ly6G, NIMP and S100 calcium-binding protein A9 (S100A9), was suppressed in the *Cxcr2 flox* bladder stroma compared to those in the *wildtype* (p=0.004) (Figure 2A, B). Similarly, infiltration of $F4/80^+$ macrophages were also downregulated as expected (p=0.004) (Figure 2D). Furthermore, TILs, including $CD3^+$, Granzyme B^+ (GrB^+), $CD4^+$, and $FoxP3^+$ cells, was significantly reduced in the *Cxcr2 flox* bladder stroma (Figure

2F). Similar changes were observed throughout the bladder tissue, including the urothelium and the bladder muscle (Figure S2).

At 16 weeks, reduced infiltration of neutrophils and T cells was observed (Figure 2A, F, S2), likely to be in reflection of the cessation of carcinogen at 10-week time point. Interestingly, however, a significant increase in macrophages was observed in the *Cxcr2 flox* bladder stroma compared to *wildtype* (p=0.029) (Figure 2D, E). At 20 weeks, infiltration of $Ly6G^+$ and $S100A9^+$ neutrophils was continued to be suppressed in *Cxcr2 flox* tumours compared to *wildtype* (p=0.039, 0.048, respectively, Figure 2A, C), while levels of macrophages remained low (Figure 2D). Unexpectedly, overall levels of TILs were higher in *Cxcr2 flox* mice compared to *wildtype* ($CD3^+$, p=0.049. Figure 2F). TILs were mostly observed in the tumour stroma, as shown in the example of $CD3^+$ cells (Figure 2G).

We then investigated how genotype and tumour phenotype are correlated with immune cell levels. Cross-examining the relationship between genotype, phenotype and immune cell infiltrations observed in each sample (Figure S3), genotype was associated with infiltrating immune cells at 2 weeks as expected. At 20 weeks, association between genotype remained with Ly6G and CD3 levels, with little association between tumour phenotype and TILs, indicating that *Cxcr2* deletion is more likely to have influenced the changes in the level of $CD3^+$ T cells at 20 weeks rather than the tumour phenotype.

Finally, to see how changes in the immune cell levels have influenced the tumour burden, we analysed the status of cell proliferation and apoptosis in tumour tissues at 20 weeks (Figure 2H-K). $Ki67^+$ proliferating cells were observed mostly in the basal edge of *CIS* and in tumours (Figure 2H). Levels of $Ki67^+$ cells were similar in *wildtype* and *Cxcr2 flox* tumours

(Figure 2I), indicating that the increased tumour burden in *Cxcr2 flox* may have originated at an earlier stage. Caspase 3^+ cells were relatively infrequent in tumours of both genotypes (Figure 2J). No significant difference was observed in the density of Caspase 3^+ cells in *wildtype* and *Cxcr2 flox* tumours (Figure 2K). No obvious similarity was found in the location of Caspase3^+ cells with those of Ly6G$^+$ neutrophils or TILs (Figure 2C, G, J).

Taken together, following a transient increase of macrophages at the outset of tumour formation, an increase in T cell infiltration was observed in *Cxcr2 flox* tumours. However, the elevated level of TILs was not associated with changes in cell proliferation or cell death in the absence of *Cxcr2*. Therefore, the increased tumour burden upon *Cxcr2* deletion may have resulted from a suppression of acute inflammation in the bladder at the time of tumour initiation.

Levels of blood immune cells did not always correlate with those in the bladder tissue

The effects of *Cxcr2* deletion on blood leukocyte populations were compared to those in the tissues (Figure S4). At 2 weeks from the start of OH-BBN treatment, the level of neutrophils in the blood appeared lower in *Cxcr2 flox* mice compared to *wildtype*, as expected, while basophils appeared to have increased (Figure S4A, B, not statistically significant). At 16 weeks, the blood levels of monocytes were higher in *Cxcr2 flox* mice (p=0.016) (Figure S4B), similar to the observations in the tissue (Figure 2B). In addition, the lower population of neutrophils within the whole blood (p=0.024, Figure S4A), and higher blood concentration of lymphocytes were observed (p=0.032, Figure S4B), leading to the lower NLR value (p=0.032, Figure S4A, B). While this was not detected in the tissue level at 16 weeks, it resembled the observations in the tumour tissue at 20 weeks (Figure 2A, F).

In contrast, the lower densities of tissue-infiltrating neutrophil and the higher TILs observed in *Cxcr2 flox* compared to *wildtype* (Figure 2A, F) were not detected in the blood in tumour-bearing mice at 20 weeks (Figure S4A, B). Instead, the higher monocyte and lower lymphocyte concentrations were observed in the blood in non-tumour bearing *Cxcr2 flox* mice compared to *wildtype* (Figure S4B).

Finally, tumour-bearing mice showed higher levels of neutrophils, NLR, and eosinophils, compared to non-tumour bearing mice in *wildtype* (p=0.028, 0.049, 0.025, respectively) (Figure S4B). This indicated that, in contrast to the findings in the tissue, the presence of tumours had more effects on granulocyte and lymphocyte levels in circulation, and that it confirms the association of higher NLR values with worse prognosis in terms of tumour presence.

Taken together, the levels of immune cells in the blood did not always correspond with those in the bladder tissue. Interestingly, changes may have occurred in a specific population of granulocytes depending on the stage of tumour pathogenesis.

Both low and high CXCR2 expression ranges are associated with a poor prognosis in human bladder cancer

To elucidate the role of CXCR2 in human bladder cancer, we analysed the data available from TCGA Bladder Cancer (Cell 2017) cohort (n=412) [32]. The OncoPrinter function in the cBioPortal revealed that *CXCR2* deletions occurred in 8 samples (n=8/404, 2.0%) together with deletions of *CXCR1* (n=8/8) and those of chemokine receptor *CCR2* (n=2/8) (Figure S5A, B). Interestingly, deletions of *CXCR2* occurred together with those of T cell inhibitors,

PD-1 (n=6) and *CTLA4* (n=3) (Figure S5C), however mostly mutually exclusive with genomic alterations common in bladder cancer, such as *FGFR3* and *TP53* (Figure S5D). By Spearman correlation analysis, we found that the level of *CXCR2* mRNA was inversely correlated with age, disease stage, metastatic stage, histological grade and mutation count (Figure S6A). *CXCR2* was not associated with specific MIBC molecular subtype, unlike the example of *FGFR3* that is associated with luminal papillary subtype [32, 37] (Figure S6B).

Kaplan-Meier analysis showed a worse overall survival associated with a lower level of *CXCR2* mRNA expression, with a median survival of 32.0 months, in contrast to 92.9 months in patients with higher expression (log-rank, p=0.044) (Figure 3A). Previous studies, however, mostly reported the pro-tumour role associated with an increase of CXCR2 signalling [25, 26, 28, 38, 39], including those in bladder cancer [29-31]. Investigating the highest level of *CXCR2* mRNA (≥80 log2 expression), we found that the median survival was 46.8 months, while 97.0 months in the medium range of CXCR2 mRNA (≥40, <80 log2 expression) (Figure S7A). *CXCR2* expression was positively associated with the levels of *CXC* ligands, including *CXCL1*, *CXCL6* and *CXCL8*, in both $CXCR2^{low}$ (<40 log2 expression) and $CXCR2^{high}$ (≥80 log2 expression) ranges (Figure 3B, S7B). Interestingly, in the $CXCR2^{low}$ group, *PD-L1* expression level was inversely correlated with *CXCR2* expression (Spearman r -0.124, p=0.041). In contrast, in the $CXCR2^{high}$ group, the correlation was positive (Spearman r 0.281, p=0.023) (Figure 3C, S7), which is in line with the previous studies where increased *CXCR2* expression was associated with an immune suppressive, pro-tumour role.

Status of immune suppression in the OH-BBN treated mice

To better understand how the above observations in human bladder cancer reflect in our mouse model, we examined the expression of regulatory genes in inflammation and immunity using an RNA array approach. Upregulation was observed in both immunostimulatory and immunosuppressive factors in *Cxcr2 flox* tumours comparing to *wildtype* tumours at 20 weeks (n=3 *wildtype*, n=2 *Cxcr2 flox*) (Table S3), including that of a pro-inflammatory factor, *interferon γ* (*Ifn*g), as well as immunosuppressive factors produced by regulatory T cells, *Transforming growth factor β* (*Tgfβ*) and *interleukin 10* (*Il10*). *Pcdc-1/Pd-1 and Cd274/Pd-L1* were also upregulated (4.55 and 2.84 log2 fold, respectively) in the absence of *Cxcr2*. Interestingly, *Ccr2*, a chemokine receptor that plays a major role in monocyte chemotaxis [40], and its ligand *Ccl2*, were highly upregulated in *Cxcr2 flox* tumours (6.68 and 3.16 log2 fold, respectively).

As our current OH-BBN model is optimised for the evaluation of tumour formation and initial tumour pathogenesis, it is possible that tumours had not been allowed to develop long enough to acquire a strong immunosuppressive tumour microenvironment. To assess whether immune suppression could be developed in the tumour microenvironment of our OH-BBN model, we quantified the density of $Ly6G^+$ neutrophils, $F4/80^+$ macrophages and TILs in tumour-bearing *wildtype* mice, at later timepoints, up to 43 weeks from the start of the carcinogen treatment (Figure 3D). The majority of $F4/80^+$ macrophages were observed in the stroma and rarely observed in tumours at 20 weeks and the timepoints beyond (Figure 2B and data not shown). Longer timepoints were associated with fewer $Ly6G^+$, $CD3^+$ and $CD8^+$ cells, but not with tumour area size (Figure 3E). Tumour area size was not corelated with immune cell densities (Figure S8A). In contrast, a higher density of $Ly6G^+$ cells was associated with a higher overall populations of TILs (Figure 3F), indicating that $Ly6G^+$ neutrophils remained to bear an anti-tumour role, being populated together with T cells in tumours.

Taken together, our OH-BBN-induced *Cxcr2 flox* mouse model may reflect human bladder cancer whereby *CXCR2* expression is low, in terms of worse disease prognosis, and an elevated level of immunosuppressive factors, such as *Pd-1/Pd-L1*. The status of immune suppression in *Cxcr2 flox* mice remained ambiguous, as upregulation was found in both immunostimulatory and immunosuppressive factors. However, it is unlikely that tumours in our current OH-BBN model developed an immunosuppressive tumour microenvironment, in which myeloid cells turned pro-tumour and suppressed T cell functions.

DISCUSSION

In this study, we showed that the loss of *Cxcr2* in myeloid cells promoted bladder tumour progression, evidenced by a robust enhancement of earlier and frequent tumour phenotype in the *Cxcr2 flox* mice (Figure 1, Figure S1, Figure S8B). Despite an increase in TILs (Figure 2), the increased tumour burden in *Cxcr2 flox* mice resulted largely independently of their cytotoxic function (Figure 2). Instead, this tumour phenotype may have resulted from a suppression of acute inflammation in the bladder in the absence of *Cxcr2* at the time of tumour formation. Our *Cxcr2 flox* model reflected the worse prognosis associated with the $CXCR2^{low}$ expression range in TCGA MIBC cohort (Figure 3).

CXCR2 is reported to be expressed mainly in myeloid cell lineage, including neutrophils, monocytes, macrophage, and mast cells [25, 26]. Therefore, a reduced recruitment of neutrophils and macrophages to the bladder in response to OH-BBN at 2-weeks timepoint (Figure 2) was expected in a model of *Cxcr2* loss. In addition, the level of T populations was also reduced (Figure 2). Single Cell Type data in Human Protein Atlas, proteinatlas.org [36]

indicates that *CXCR2* is also present in T cells. In the *LysMCre* mice used in the study, efficiency of *Cre-lox* recombination was previously shown in the majority of neutrophils and macrophages, but little recombination was reported in B and T cells [33]. Therefore, the reduction of T cells is not caused directly by the loss of *Cxcr2,* but likely to be secondary to the changes in myeloid cells.

We have observed a transient increase in macrophage infiltration in *Cxcr2 flox* bladders at the onset of tumour formation (Figure 2D). The increase of macrophages may be a part of the compensatory signalling in the absence of *Cxcr2*. Indeed, expression of *Ccr2,* which is mainly expressed in monocytes and macrophages, and its ligand *Ccl2,* was highly upregulated in *Cxcr2 flox* tumours comparing to *wildtype* (Table S3). This is consistent with the report in which *Cxcr2*$^{-/-}$ mice showed an increase in macrophage infiltration at the acutely inflamed sites with exaggerated cutaneous inflammation [41], and in a model of pancreatic adenocarcinoma, where inhibition of Cxcr2 led to an increase of TAM, while inhibition of Ccr2 and TAM infiltration lead to an increase of tumour infiltrating neutrophils [40].

The levels of immune cells in the blood circulation and those of tissue-infiltrating immune cells were not always comparable (Figure 2, Figure S4). Consequences of *CXCR2* deletion in the bone marrow may appear in the blood more directly, rather than in the tissues where infiltrations could be regulated by the microenvironment. An increase in monocytes in *Cxcr2 flox* mice in the blood at 16 weeks (Figure S4) was reflected in the tissue (Figure 2D). However, an increase in monocytes at 20 weeks was observed in non-tumour bearing mice (Figure S4), therefore unlikely to have been caused by tumour phenotype. Instead, the increase in blood monocyte levels may have occurred in compensation to the earlier suppression of acute inflammation by *Cxcr2* deletion. The predictive value of NLR was only

valid comparing tumour-bearing and non-tumour bearing mice at 20 weeks (Figure S4). The blood analysis also indicated that basophils may have increased at 2 weeks and that there was a significant upregulation of eosinophils in tumour-bearing mice comparing to non-tumour bearing mice at 20 weeks (Figure S5), suggesting granulocyte-specific changes depending on a disease stage.

Multiple types of myeloid cells, including neutrophils, monocytes and MDSCs, could influence the tumour microenvironment [9-13, 21-23]. Tumour-infiltrating myeloid cells were shown to account for 10-20% of cells found in bladder tumour tissues, and that 30-40% were granulocytic or polymorphonuclear (G/PMN)-MDSCs in both non-invasive and invasive tumours, with the rest being monocytic (M)-MDSCs [42]. In benign conditions, MDSCs contribute to homeostasis of T cell-mediated inflammatory response, however, in cancer, G/PMN-MDSC and M-MDSC are both immune suppressive [9, 43]. Triggered by chronic inflammation or malignancy, MDSCs induce immunosuppression, by producing, for example, inhibitory cytokines and TGFβ, and inhibiting IFNγ-mediated proinflammatory signals. High MDSC is associated with worse prognosis and poor response to BCG, chemo- and ICI therapy in bladder cancer [43]. Pro-tumour CXCR2 signalling in bladder cancer has so far been attributed to its expression in immunosuppressive MDSCs [30, 31]. A higher proportion of cells were *CXCR2*$^{+}$ in MDSCs in patients' tumours than those in the peripheral blood [30]. *Cxcr2* was also overexpressed in MDSCs in mice with MB49 tumours as well as those with chemo-resistant MB49B [31]. Upon close examination of TCGA Bladder Cancer (Cell 2017) dataset, we have shown that both *CXCR2*^{low} and *CXCR2*^{high} expression ranges is associated with poor prognosis and increased *PD-L1* expression (Figure 3, S7). We speculate that the *CXCR2*^{low} cases are reflected in our mouse model, and *CXCR2*^{high}, the previous reports of *CXCR2* overexpression [30, 31].

The pro-tumour role of CXCR2 was reported previously in colon cancer [44], breast cancer [45], rhabdomyosarcoma [27], and pancreatic ductal adenocarcinoma [28, 46]. The role of CXCR2 could also differ dependent on tissue types and the stages of tumour progression. In an early stage of lung cancer, a subset of tumour infiltrating neutrophils showed antigen-presenting cell (APC)-like characteristics and was able to activate T cell proliferation and IFNγ release, therefore not immunosuppressive [47, 48]. The anti-tumour role of CXCR2 could be mediated by re-enforcement of oncogene-induced senescence in tumour cells [49, 50]. A possibility that *Cxcr2* deleted in myeloid cells have perturbated the autocrine chemokine signalling in tumours, influencing the senescence-associated secretory phenotype, cannot be excluded.

The limitations of the current study are as follows. Firstly, the current OH-BBN protocol is restricted to model early-stage tumours and tumour microenvironment remained immune competent, with tumour-infiltrating neutrophils maintaining a positive correlation with TIL density (Figure 3F). Therefore, the role of CXCR2 in an immune suppressive environment and in metastasis cannot be assessed [9, 11, 13](Figure S8B). Secondly, the study was conducted with a genetically modified mouse model, and the frequency and size of the tumours were not sufficiently large to allow characterization of myeloid cell populations by flow cytometry and cytokine expression by ELISA. Finally, deletion or pharmacological inhibition of *Cxcr2* in mice led to an enhanced T cell infiltration in the tumour in pancreatic ductal carcinoma [28]. While a similar elevated level of TILs was observed in *Cxcr2 flox* tumours (Figure 2F), our current model does not provide evidence that supports such modulation to sensitize bladder tumours to ICIs. Mechanistic understanding of tumour immune microenvironment requires suitable models that reflect the advanced status of tumour

progression and immune suppression. In such models, the status of CXCR2 and myeloid cell diversity could be further investigated for their influence in regulating response towards PD-1/PD-L1 inhibitors. The use of CXCR2 inhibitors requires a cautious approach and should be investigated together with a marker that indicates the status of immune suppression in invasive urothelial carcinoma.

ACKNOWLEDGEMENTS

We thank Biological and Histology Services at Cancer Research UK Beatson Institute for their technical support, Dr Catherine Winchester for editing the manuscript. We are grateful to Dr Seth Coffelt and Professor Owen J. Sansom, for insights in neutrophil biology and for project conception and support, respectively. We also thank Professor Margaret A Knowles, St James's University Hospital, for helpful discussions and encouragement.

FUNDING

This work was funded by Public Department of Malaysia (NFBI), Ministry of Higher Education of Libya (AREY), MRC MR/N021800/1 (JDGL), CRUK A17196 and A31287 core funding to the Beatson Institute (TJ, SAK, JPM), CRUK A21139 core funding to Sansom lab (TJ), and CRUK A29996 core funding to JPM lab (JPM).

AUTHOR CONTRIBUTIONS

Conception: NFBI, MF, JPM, TI; Performance of work: NFBI, MF, AREY, NC, TJ, SAK, TI; Interpretation of analysis of data: NFBI, MF, AREY, NC, JDGL, TJ, SAK, JMS, JPM, TI; Writing of the article: NFBI, JPM, TI. All authors critically reviewed and edited the manuscript drafts.

CONFLICT OF INTEREST

No conflicts of interest were declared by NFBI, MF, AREY, NC, JDGL, TJ, SAK, JMS, JPM, and TI.

SUPPLEMENTARY MATERIAL

Supplementary Tables S1-S3 and Supplementary Figures S1-S8 are available in the electronic version of this article.

REFERENCES

[1] Richters A, Aben KKH, Kiemeney L. The global burden of urinary bladder cancer: an update. World journal of urology. 2020;38:1895-904.

[2] Saginala K, Barsouk A, Aluru JS, Rawla P, Padala SA, Barsouk A. Epidemiology of Bladder Cancer. Med Sci (Basel). 2020;8.

[3] Tran L, Xiao JF, Agarwal N, Duex JE, Theodorescu D. Advances in bladder cancer biology and therapy. Nat Rev Cancer. 2021;21:104-21.

[4] Babjuk M, Bohle A, Burger M, Capoun O, Cohen D, Comperat EM, et al. EAU Guidelines on Non-Muscle-invasive Urothelial Carcinoma of the Bladder: Update 2016. Eur Urol. 2017;71:447-61.

[5] Alfred Witjes J, Lebret T, Comperat EM, Cowan NC, De Santis M, Bruins HM, et al. Updated 2016 EAU Guidelines on Muscle-invasive and Metastatic Bladder Cancer. Eur Urol. 2017;71:462-75.

[6] Siefker-Radtke A, Curti B. Immunotherapy in metastatic urothelial carcinoma: focus on immune checkpoint inhibition. Nature reviews Urology. 2018;15:112-24.

[7] Song D, Powles T, Shi L, Zhang L, Ingersoll MA, Lu YJ. Bladder cancer, a unique model to understand cancer immunity and develop immunotherapy approaches. The Journal of pathology. 2019;249:151-65.

[8] Lopez-Beltran A, Cimadamore A, Blanca A, Massari F, Vau N, Scarpelli M, et al. Immune Checkpoint Inhibitors for the Treatment of Bladder Cancer. Cancers (Basel). 2021;13.

[9] Coffelt SB, Wellenstein MD, de Visser KE. Neutrophils in cancer: neutral no more. Nat Rev Cancer. 2016;16:431-46.

[10] Powell DR, Huttenlocher A. Neutrophils in the Tumor Microenvironment. Trends Immunol. 2016;37:41-52.

[11] Leach J, Morton JP, Sansom OJ. Neutrophils: Homing in on the myeloid mechanisms of metastasis. Mol Immunol. 2019;110:69-76.

[12] Mackey JBG, Coffelt SB, Carlin LM. Neutrophil Maturity in Cancer. Front Immunol. 2019;10:1912.

[13] Masucci MT, Minopoli M, Carriero MV. Tumor Associated Neutrophils. Their Role in Tumorigenesis, Metastasis, Prognosis and Therapy. Front Oncol. 2019;9:1146.

[14] Mandelli GE, Missale F, Bresciani D, Gatta LB, Scapini P, Caveggion E, et al. Tumor Infiltrating Neutrophils Are Enriched in Basal-Type Urothelial Bladder Cancer. Cells. 2020;9.

[15] Zhou L, Xu L, Chen L, Fu Q, Liu Z, Chang Y, et al. Tumor-infiltrating neutrophils predict benefit from adjuvant chemotherapy in patients with muscle invasive bladder cancer. Oncoimmunology. 2017;6:e1293211.

[16] Liu K, Zhao K, Wang L, Sun E. The prognostic values of tumor-infiltrating neutrophils, lymphocytes and neutrophil/lymphocyte rates in bladder urothelial cancer. Pathol Res Pract. 2018;214:1074-80.

[17] Kawahara T, Furuya K, Nakamura M, Sakamaki K, Osaka K, Ito H, et al. Neutrophil-to-lymphocyte ratio is a prognostic marker in bladder cancer patients after radical cystectomy. BMC Cancer. 2016;16:185.

[18] Kaiser J, Li H, North SA, Leibowitz-Amit R, Seah JA, Morshed N, et al. The Prognostic Role of the Change in Neutrophil-to-Lymphocyte Ratio During Neoadjuvant Chemotherapy in Patients with Muscle-Invasive Bladder Cancer: A Retrospective, Multi-Institutional Study. Bladder Cancer. 2018;4:185-94.

[19] Vartolomei MD, Porav-Hodade D, Ferro M, Mathieu R, Abufaraj M, Foerster B, et al. Prognostic role of pretreatment neutrophil-to-lymphocyte ratio (NLR) in patients with non-muscle-invasive bladder cancer (NMIBC): A systematic review and meta-analysis. Urol Oncol. 2018;36:389-99.

[20] Black AJ, Zargar H, Zargar-Shoshtari K, Fairey AS, Mertens LS, Dinney CP, et al. The prognostic value of the neutrophil-to-lymphocyte ratio in patients with muscle-invasive bladder cancer treated with neoadjuvant chemotherapy and radical cystectomy. Urol Oncol. 2020;38:3 e17-3 e27.

[21] Leblond MM, Zdimerova H, Desponds E, Verdeil G. Tumor-Associated Macrophages in Bladder Cancer: Biological Role, Impact on Therapeutic Response and Perspectives for Immunotherapy. Cancers (Basel). 2021;13.

[22] Cassetta L, Pollard JW. Targeting macrophages: therapeutic approaches in cancer. Nat Rev Drug Discov. 2018;17:887-904.

[23] Mantovani A, Marchesi F, Malesci A, Laghi L, Allavena P. Tumour-associated macrophages as treatment targets in oncology. Nat Rev Clin Oncol. 2017;14:399-416.

[24] Mora-Bau G, Platt AM, van Rooijen N, Randolph GJ, Albert ML, Ingersoll MA. Macrophages Subvert Adaptive Immunity to Urinary Tract Infection. PLoS Pathog. 2015;11:e1005044.

[25] Cheng Y, Ma XL, Wei YQ, Wei XW. Potential roles and targeted therapy of the CXCLs/CXCR2 axis in cancer and inflammatory diseases. Biochim Biophys Acta Rev Cancer. 2019;1871:289-312.

[26] Jaffer T, Ma DQ. The emerging role of chemokine receptor CXCR2 in cancer progression. Transl Cancer Res. 2016;5:S616-S28.

[27] Highfill SL, Cui Y, Giles AJ, Smith JP, Zhang H, Morse E, et al. Disruption of CXCR2-mediated MDSC tumor trafficking enhances anti-PD1 efficacy. Sci Transl Med. 2014;6:237ra67.

[28] Steele CW, Karim SA, Leach JDG, Bailey P, Upstill-Goddard R, Rishi L, et al. CXCR2 Inhibition Profoundly Suppresses Metastases and Augments Immunotherapy in Pancreatic Ductal Adenocarcinoma. Cancer Cell. 2016;29:832-45.

[29] Gao Y, Guan Z, Chen J, Xie H, Yang Z, Fan J, et al. CXCL5/CXCR2 axis promotes bladder cancer cell migration and invasion by activating PI3K/AKT-induced upregulation of MMP2/MMP9. Int J Oncol. 2015;47:690-700.

[30] Zhang H, Ye YL, Li MX, Ye SB, Huang WR, Cai TT, et al. CXCL2/MIF-CXCR2 signaling promotes the recruitment of myeloid-derived suppressor cells and is correlated with prognosis in bladder cancer. Oncogene. 2017;36:2095-104.

[31] Takeyama Y, Kato M, Tamada S, Azuma Y, Shimizu Y, Iguchi T, et al. Myeloid-derived suppressor cells are essential partners for immune checkpoint inhibitors in the treatment of cisplatin-resistant bladder cancer. Cancer Lett. 2020;479:89-99.

[32] Robertson AG, Kim J, Al-Ahmadie H, Bellmunt J, Guo G, Cherniack AD, et al. Comprehensive Molecular Characterization of Muscle-Invasive Bladder Cancer. Cell. 2017;171:540-56 e25.

[33] Clausen BE, Burkhardt C, Reith W, Renkawitz R, Forster I. Conditional gene targeting in macrophages and granulocytes using LysMcre mice. Transgenic Res. 1999;8:265-77.

[34] Bankhead P, Loughrey MB, Fernandez JA, Dombrowski Y, McArt DG, Dunne PD, et al. QuPath: Open source software for digital pathology image analysis. Sci Rep. 2017;7:16878.

[35] Foth M, Ismail NFB, Kung JSC, Tomlinson D, Knowles MA, Eriksson P, et al. FGFR3 mutation increases bladder tumourigenesis by suppressing acute inflammation. The Journal of pathology. 2018;246:331-43.

[36] Uhlen M, Fagerberg L, Hallstrom BM, Lindskog C, Oksvold P, Mardinoglu A, et al. Proteomics. Tissue-based map of the human proteome. Science. 2015;347:1260419.

[37] Sweis RF, Spranger S, Bao R, Paner GP, Stadler WM, Steinberg G, et al. Molecular Drivers of the Non-T-cell-Inflamed Tumor Microenvironment in Urothelial Bladder Cancer. Cancer Immunol Res. 2016;4:563-8.

[38] Jamieson T, Clarke M, Steele CW, Samuel MS, Neumann J, Jung A, et al. Inhibition of CXCR2 profoundly suppresses inflammation-driven and spontaneous tumorigenesis. J Clin Invest. 2012;122:3127-44.

[39] Steele CW, Karim SA, Foth M, Rishi L, Leach JD, Porter RJ, et al. CXCR2 inhibition suppresses acute and chronic pancreatic inflammation. The Journal of pathology. 2015;237:85-97.

[40] Nywening TM, Belt BA, Cullinan DR, Panni RZ, Han BJ, Sanford DE, et al. Targeting both tumour-associated CXCR2(+) neutrophils and CCR2(+) macrophages disrupts myeloid recruitment and improves chemotherapeutic responses in pancreatic ductal adenocarcinoma. Gut. 2018;67:1112-23.

[41] Dyer DP, Pallas K, Medina-Ruiz L, Schuette F, Wilson GJ, Graham GJ. CXCR2 deficient mice display macrophage-dependent exaggerated acute inflammatory responses. Sci Rep. 2017;7:42681.

[42] Eruslanov E, Neuberger M, Daurkin I, Perrin GQ, Algood C, Dahm P, et al. Circulating and tumor-infiltrating myeloid cell subsets in patients with bladder cancer. Int J Cancer. 2012;130:1109-19.

[43] Puttmann K, Duggan M, Mortazavi A, Diaz DA, Carson WE, Sundi D. The Role of Myeloid Derived Suppressor Cells in Urothelial Carcinoma Immunotherapy. Bladder Cancer. 2019;5:103-14.

[44] Yamamoto M, Kikuchi H, Ohta M, Kawabata T, Hiramatsu Y, Kondo K, et al. TSU68 prevents liver metastasis of colon cancer xenografts by modulating the premetastatic niche. Cancer Res. 2008;68:9754-62.

[45] Acharyya S, Oskarsson T, Vanharanta S, Malladi S, Kim J, Morris PG, et al. A CXCL1 paracrine network links cancer chemoresistance and metastasis. Cell. 2012;150:165-78.

[46] Chao T, Furth EE, Vonderheide RH. CXCR2-Dependent Accumulation of Tumor-Associated Neutrophils Regulates T-cell Immunity in Pancreatic Ductal Adenocarcinoma. Cancer Immunol Res. 2016;4:968-82.

[47] Eruslanov EB, Bhojnagarwala PS, Quatromoni JG, Stephen TL, Ranganathan A, Deshpande C, et al. Tumor-associated neutrophils stimulate T cell responses in early-stage human lung cancer. J Clin Invest. 2014;124:5466-80.

[48] Singhal S, Bhojnagarwala PS, O'Brien S, Moon EK, Garfall AL, Rao AS, et al. Origin and Role of a Subset of Tumor-Associated Neutrophils with Antigen-Presenting Cell Features in Early-Stage Human Lung Cancer. Cancer Cell. 2016;30:120-35.

[49] Acosta JC, O'Loghlen A, Banito A, Guijarro MV, Augert A, Raguz S, et al. Chemokine signaling via the CXCR2 receptor reinforces senescence. Cell. 2008;133:1006-18.

[50] Lesina M, Wormann SM, Morton J, Diakopoulos KN, Korneeva O, Wimmer M, et al. RelA regulates CXCL1/CXCR2-dependent oncogene-induced senescence in murine Kras-driven pancreatic carcinogenesis. J Clin Invest. 2016;126:2919-32.

Table 1. Summary of the mouse cohorts.

Genotype	Time from the start of OH-BBN treatment (weeks)	Cohort size (n)			Haematuria (n)		Tumour incidents observed by histopathology (n)	
		Total	Male	Female	Male	Female	Male	Female
LysMCre Cxcr2$^{flox/flox}$ (Cxcr2 flox)	2	41	29	12				
	16	5	5	0				
	20	43	27	16	8/27 (29.6%)	0/16 (0%)	15/27 (55.6%)	6/16 (37.5%)
Wildtype	2	37	28	9				
	16	5	5	0				
	20	72	45	27	0/45 (0%)	0/27 (0%)	16/45 (35.6%)	1/27 (3.7%)
	>20w	10	10		2/10 (20%)		10/10 (100%)	

Mice were monitored for general health and clinical signs of bladder cancer, including haematuria, difficulties in micturition and weight loss. Haematuria was notable in *Cxcr2 flox* males at 20 weeks. None of the mice presented haematuria or tumours at 2 and 16 weeks. *Wildtype* mice aged beyond 20 weeks (21 – 43 weeks) were monitored by ultrasound imaging for bladder tumours and culled when mice showed clinical signs of bladder tumours. Data of *wildtype* mice at 2 and 20 weeks from our previous study [35] were included.

Figure legends

Figure 1. Bladder tumour phenotype of *LysMCre Cxcr2*$^{flox/flox}$ (*Cxcr2 flox*) mice. (**A**) Mice were given tobacco carcinogen 0.05% (v/v) OH-BBN in drinking water for 10 weeks, and bladder tissues were examined at 2, 16 and 20 weeks from the start of the carcinogen treatment. (**B**) An example of a bladder tumour developed at 20 weeks from the start of the carcinogen treatment in a *Cxcr2 flox* animal, with an invasion to the muscle (arrow) and keratinization (Kr). Representative images of *wildtype* (**C, E**) and *Cxcr2 flox* (**D, F**) bladders at 16 weeks (**C, D**), and 2 weeks (**E, F**). Enhanced tumour pathogenesis of the urothelium, such as carcinoma *in situ*-like lesions (arrowheads) was observed in *Cxcr2 flox* bladders at 16 weeks (D). At 2 weeks, the differences between *wildtype* and *Cxcr2 flox* bladders were not evident. IHC staining showed infiltrating Cxcr2^{+} myeloid cells in tumours at 20 weeks (**G**), the urothelium (**J**) and around the blood vessels in the bladder stroma (**L**) at 2 weeks in *wildtype* mice (arrows in G, J, L). In contrast, the staining was absent in *Cxcr2 flox* tumours (**H, I**) and in the bladder at 2 weeks' time point (**K, M**). IHC staining was performed in at least n=3 samples in each genotype. Annotations in B-M are; *CIS*, carcinoma *in situ*; Kr, keratinization; M, muscle, St, stroma; T, tumour; U, urothelium; V, blood vessel. The scale bar represents 500 μm in B, 250 μm in C-F, 30 μm in G-M. For evaluation of the bladder and tumour phenotype, the scoring criteria from our previous study [35] were refined to optimally capture the phenotype of OH-BBN treated mice under our protocol. The "bladder phenotype" defines the overall state of the urothelial tumorigenesis and progression. The "invasiveness" describes the state of the basement membrane and invasion of tumour cells, while the "squamous transformation" describes the squamous appearance of cells and keratinization in the urothelium or in the tumour. The criterium "minimal changes" of the bladder phenotype was established to indicate the baseline appearance of the urothelium treated with OH-BBN

observed [35]. One representative H&E section was scored per animal. The bladders usually showed a mixed phenotype of all criteria. The worst score was used. Bladder phenotype (**N, R**), invasiveness (**O, S**) and squamous transformation (**P**) are expressed as a frequency of observations (%) comparing *wildtype* (wt, n=45) and *Cxcr2 flox* (flox, n=27) male mice at 20 weeks (N-P) and at 16 weeks (n=5 per cohort) (R, S). Incidents of tumour in N were presented by numbers in Table 1. The tumour area was measured by QuPath in a representative section per mouse at 20 weeks (n=15 per cohort) (**Q**) and carcinoma *in situ (CIS)* and tumour areas at 16 weeks (n=5 per cohort) (**T**). The means with standard deviation are shown in bars (Q, T). Observations in male mice are presented (N-T). The *p*-values (Mann-Whitney test) are indicated where significant ($p < 0.05$).

Figure 2. Suppression of Ly6G$^+$ neutrophil infiltration in *Cxcr2 flox* mouse bladders, with upregulation of macrophages at 16 weeks and CD3$^+$ T cells at 20 weeks. Populations of neutrophils (**A-C**), macrophages (**D, E**) and T cells (**F, G**) were characterised in the bladder stroma at 2 and 16 weeks, and in the tumour of *wildtype* (wt) and *Cxcr2 flox* (flox) mice at 20 weeks from the start of OH-BBN treatment. IHC markers used were Ly6G, NIMP, S100A9 and MPO for neutrophils, F4/80 for macrophages, CD3, CD8, Granzyme B (GrB), CD4, and FoxP3, for general, cytotoxic, activated, helper, and regulatory T cells, respectively. (**A, D, F**) Density of each population was quantified. The number of samples used were; *wildtype*, n=5-7, *Cxcr2 flox* n=6-7 at 2 weeks; *wildtype*, n=3-5, *Cxcr2 flox* n=4-5 at 16 weeks; *wildtype*, n=5-8, *Cxcr2 flox* n=8-11 at 20 weeks. Male mice were analysed. The bars represent the means with standard deviation. The *p*-values are indicated where significant ($p < 0.05$). Kruskal-Wallis test were used to evaluate differences in immune infiltrations during time course (indicated at the top of each graph). The differences between *Cxcr2 flox* and *wildtype* at the same timepoint were evaluated by Mann-Whitney test (indicated above each value). Images

are representative of $Ly6G^+$ neutrophils in tumours at 2 weeks (**B**) and 20 weeks (**C**), $F4/80^+$ macrophages in the bladder tissue stroma at 16 weeks (**E**), and $CD3^+$ T cells in tumours at 20 weeks (**G**), with arrowheads indicating the positively stained cells. (**H**) A similar pattern of $Ki67^+$ cells (arrowheads) were found in *CIS* and tumours in *wildtype* and *Cxcr2 flox* mice at 20 weeks. (**I**) Density of $Ki67^+$ cells were quantified in *wildtype* (n=5) and *Cxcr2 flox* tumours (n=4). (**J**) A representative image of Caspase 3 IHC staining showing the positive cell (black arrowhead) and a necrotic area (red arrowhead) in *wildtype* mice at 20 weeks. (**K**) Density of Caspase 3+ cells were quantified in *wildtype* (n=5) and *Cxcr2 flox* tumours (n=4). Scale bars indicate 50 um in B, I, K, 100 µm in C, E, and G. 100 µm and 50 µm in images of *CIS* and tumours, respectively (I)

Figure 3. Low *CXCR2* mRNA expression is associated with poor overall survival in human bladder cancer. (**A**) Kaplan-Meier survival analysis was performed using a bladder cancer dataset (TCGA , Cell 2017) with information on *CXCR2* mRNA expression and overall survival (n=400), categorised according to low (<40 log2 mRNA expression, n=269), and high (≥40 log2 mRNA expression, n=131) *CXCR2* mRNA expression (log2). (**B, C**) Using the MIBC cases of the Bladder Cancer, TCGA, Cell 2017 cohort (>T2, n=398), correlation between *CXCR2* and CXC ligands, and that of *PD-1/PD-L1* was analysed. The mRNA expression of *CXCR2* and *CXCL1, CXCL6* and *CXCL8* were positively correlated (**B**). The mRNA expression of *CXCR2* and *PD-L1* were inversely correlated in the *CXCR2* "low" range (<40 log2 mRNA expression, n=269), while positively correlated in the *CXCR2* "high" range (≥80 log2 mRNA expression, n=65) (**C**). (**D**) Mice aged beyond 20 weeks (21 – 43 weeks) were monitored by ultrasound imaging for the presence of bladder tumours and culled when mice showed clinical signs of bladder tumour, such as haematuria and weight loss. (**E**) Relationship between the timepoint of tumour development and tumour area size, as well as

immune cell density was evaluated by Spearman correlation in *wildtype* mice that developed tumour at 20 weeks (n=12) and beyond 20 weeks (n=10) from the start of OH-BBN treatment. *wildtype* mice were treated with 0.05% OH-BBN for 10 weeks. Mice aged beyond 20 weeks (21 – 43 weeks) were monitored by ultrasound imaging for the presence of bladder tumours and culled when mice showed clinical signs of bladder tumour, such as haematuria and weight loss. (**F**) The status of immune cell infiltration was evaluated using Spearman correlation between $Ly6G^+$ neutrophil density and T cell populations positive with $CD3^+$, $CD8^+$, Granzyme B^+, and $FoxP3^+$ in tumours as in **E**.

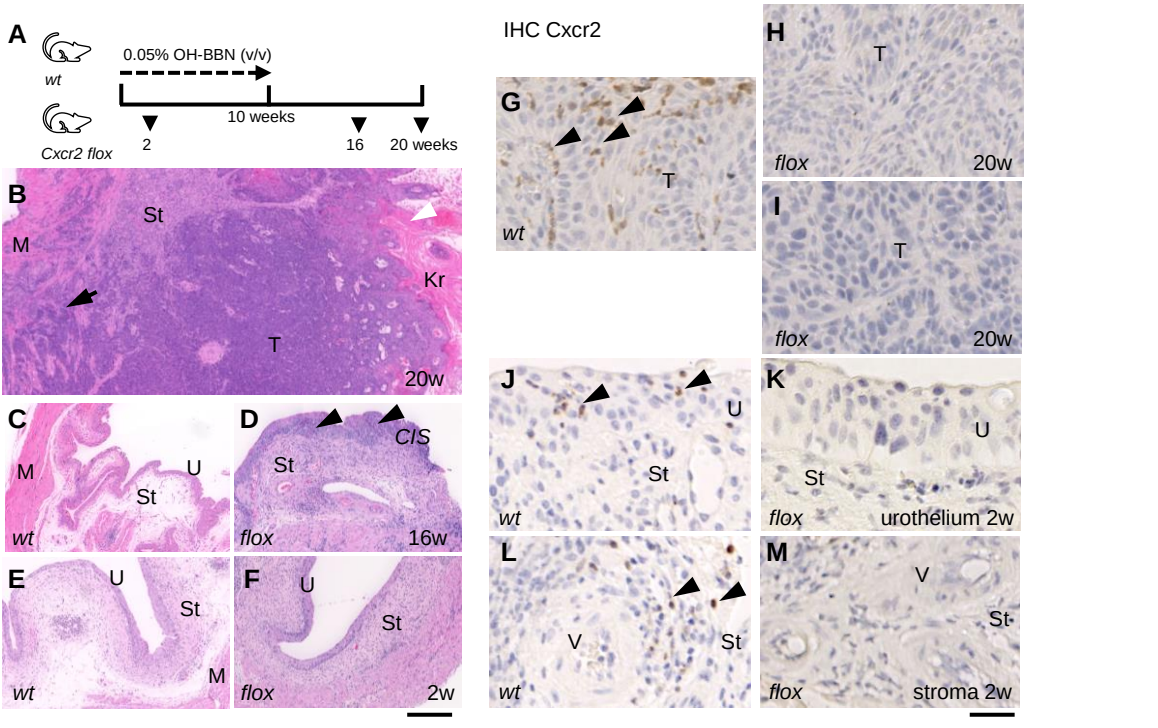

20 weeks (male)

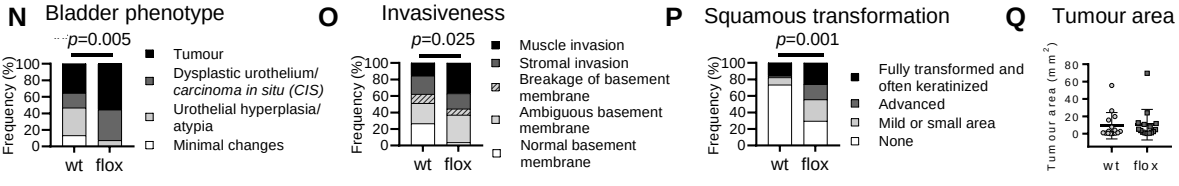

16 weeks (male)

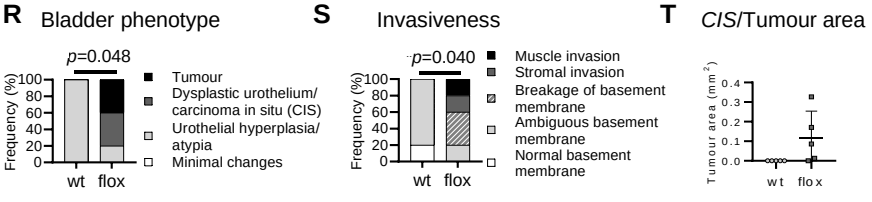

Figure 1

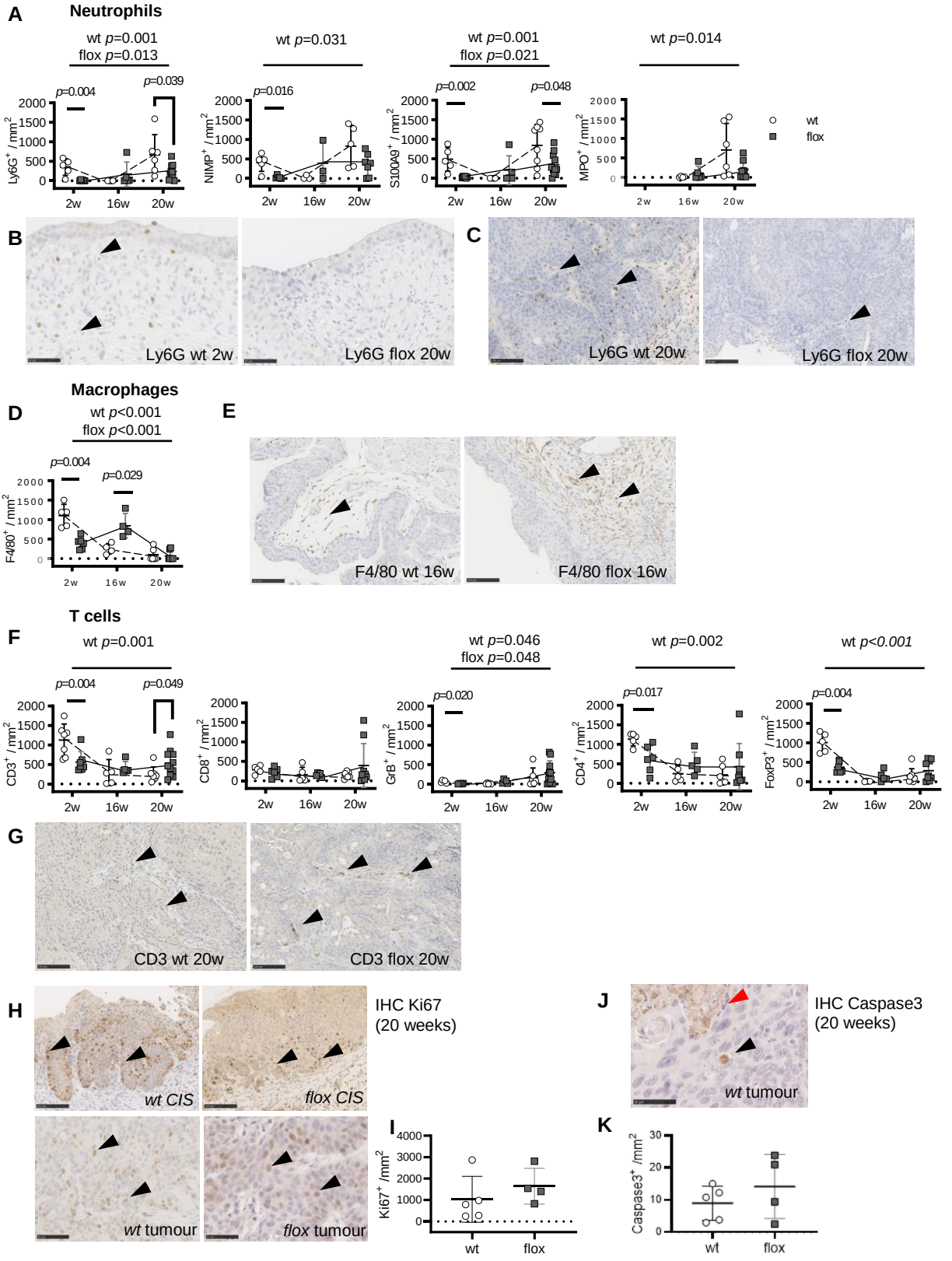
A
Neutrophils
wt p=0.001
flox p=0.013
p=0.004
p=0.039
Ly6G+ / mm2
wt p=0.031
p=0.016
NIMP+ / mm2
wt p=0.001
flox p=0.021
p=0.002
p=0.048
S100A9+ / mm2
wt p=0.014
MPO+ / mm2
wt
flox
2w
16w
20w
B
Ly6G wt 2w
Ly6G flox 20w
C
Ly6G wt 20w
Ly6G flox 20w
Macrophages
D
wt p<0.001
flox p<0.001
p=0.004
p=0.029
F4/80+ / mm2
E
F4/80 wt 16w
F4/80 flox 16w
T cells
F
wt p=0.001
p=0.004
p=0.049
CD3+ / mm2
CD8+ / mm2
wt p=0.046
flox p=0.048
p=0.020
GrB+ / mm2
wt p=0.002
p=0.017
CD4+ / mm2
wt p<0.001
p=0.004
FoxP3+ / mm2
G
CD3 wt 20w
CD3 flox 20w
H
wt CIS
flox CIS
wt tumour
flox tumour
IHC Ki67
(20 weeks)
I
Ki67+ /mm2
wt
flox
J
wt tumour
IHC Caspase3
(20 weeks)
K
Caspase3+ /mm2
wt
flox

Figure 2

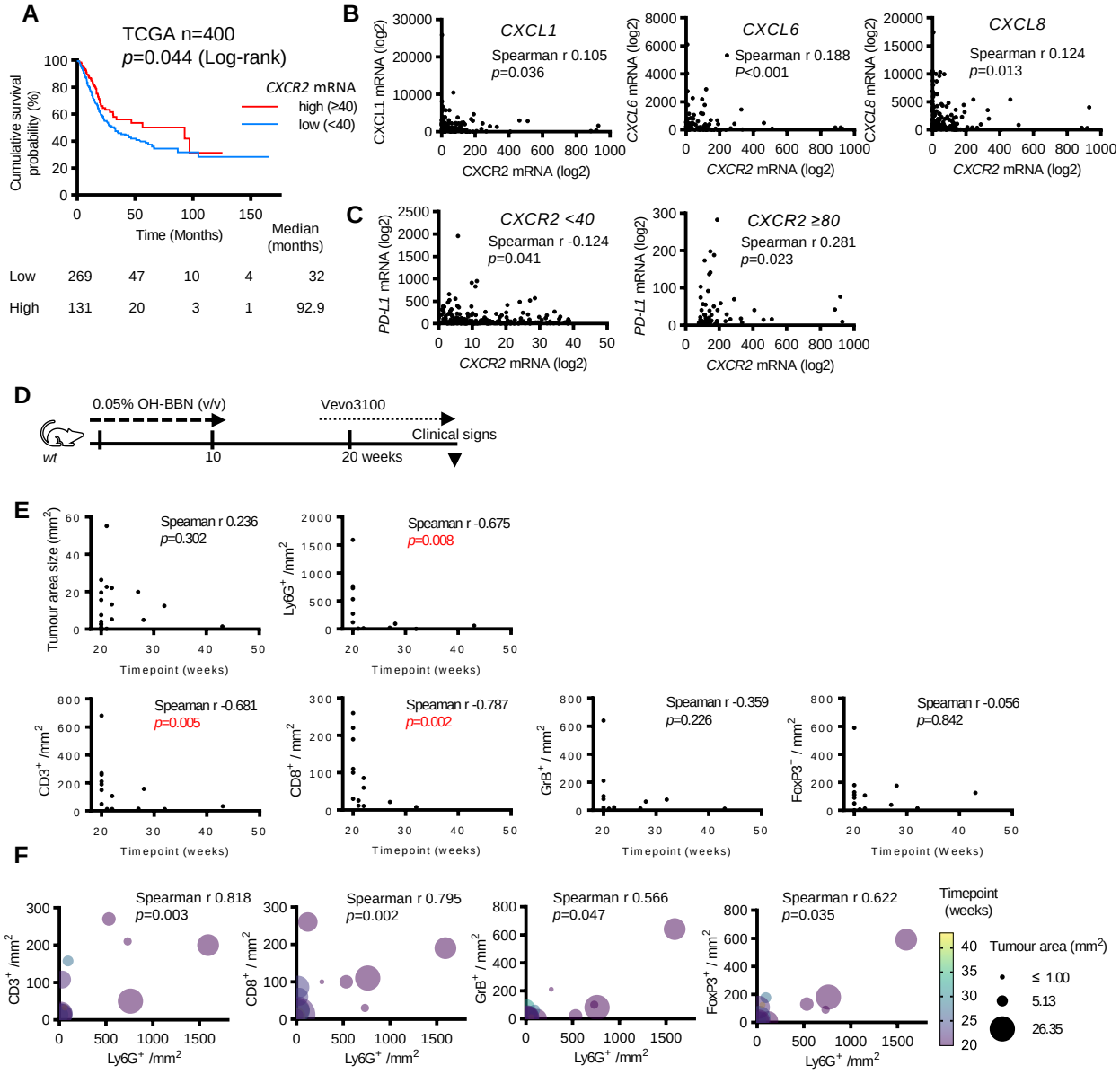
A
TCGA n=400
p=0.044 (Log-rank)
CXCR2 mRNA
high (≥40)
low (<40)
Cumulative survival probability (%)
Time (Months)
Median (months)
Low 269 47 10 4 32
High 131 20 3 1 92.9
B
CXCL1
Spearman r 0.105
p=0.036
CXCL1 mRNA (log2)
CXCR2 mRNA (log2)
CXCL6
Spearman r 0.188
P<0.001
CXCL6 mRNA (log2)
CXCL8
Spearman r 0.124
p=0.013
CXCL8 mRNA (log2)
C
CXCR2 <40
Spearman r -0.124
p=0.041
PD-L1 mRNA (log2)
CXCR2 mRNA (log2)
CXCR2 ≥80
Spearman r 0.281
p=0.023
D
0.05% OH-BBN (v/v)
Vevo3100
Clinical signs
wt
10
20 weeks
E
Tumour area size (mm2)
Spearman r 0.236
p=0.302
Ly6G+ /mm2
Spearman r -0.675
p=0.008
Timepoint (weeks)
CD3+ /mm2
Spearman r -0.681
p=0.005
CD8+ / mm2
Spearman r -0.787
p=0.002
GrB+ / mm2
Spearman r -0.359
p=0.226
FoxP3+ / mm2
Spearman r -0.056
p=0.842
F
Spearman r 0.818
p=0.003
Spearman r 0.795
p=0.002
Spearman r 0.566
p=0.047
Spearman r 0.622
p=0.035
Timepoint (weeks)
Tumour area (mm2)
≤ 1.00
5.13
26.35

Figure 3